A Comparative Study of Spark Plasma Sintering and Hybrid Spark Plasma Sintering of W-4.9Ni-2.1Fe heavy alloy

Mxolisi Brendon Shongwe[*][†], Saliou Diouf[*], Mondiu Olayinka Durowoju[*], Peter Apata Olubambi[*], Munyadziwa Mercy Ramakokovhu a, Babatunde Abiodun Obadele

[*]Institute for NanoEngineering Research, Tshwane University of Technology, Pretoria, South Africa, Department of Chemical, Metallurgical and Materials Engineering, Tshwane University of Technology, Pretoria, South Africa

ABSTRACT

Mixed 93W-4.9Ni-2.1Fe powders were sintered via the spark plasma sintering (SPS) and hybrid spark plasma sintering (HSPS) techniques with 30 mm and 60 mm samples in both conditions. After SPS and HSPS, the 30 mm and 60 mm alloys (except 60mm-SPS) had a relative density (>99.2%) close to the theoretical density. Phase, microstructure and mechanical properties evolution of W-Ni-Fe alloy during SPS and HSPS were studied. The microstructural evolution of the 60 mm alloys varied from the edge of the sample to the core of the sample. Results show that the grain size and the hardness vary considerable from the edge to the core of sintered sample of 60 mm sintered using conventional SPS compared to hybrid SPS. Similarly, the hardness also increased from the edge to the core. The 60 mm-HSPS alloy exhibit improved bending strength than the 60 mm-SPS, 1115 MPa and 920 MPa respectively, former being similar to the 30 mm-SPS and HSPS alloys. The intergranular fracture along the W/W grain boundary is the main fracture modes of W-Ni-Fe, however in the 60 mm-SPS alloy peeling of the grains was also observed which diminished the properties. The mechanical properties of SPS and HSPS 93W-4.9Ni-2.1Fe heavy alloys are dependent on the microstructural parameters such as tungsten grain size and overall homogeneity.

[†]Corresponding author. Tel: +27 12 382 5488, E-mail address: ShongweMB@tut.ac.za, m.shongwem@gmail.com (M.B. Shongwe, PhD).

1. Introduction

Generally, Tungsten heavy alloys (WHAs) can provide better mechanical and physical properties when compared to the conventional engineering metals and alloys. Due to this fact, WHAs can find many applications in both civil and military areas such as radiation shields, counterweight balances, kinetic energy penetrators, electrical contacts and damping devices. WHAs have high density, high strength and good ductility [1,2]. These alloys are usually fabricated by conventional powder metallurgy (PM), which consumes too much sintering time and energy [3]. The drawback associated with conventional PM techniques is that, after sintering, the resultant microstructure consists of coarsened spherical body-centered cubic (bcc) tungsten grains dispersed in a face-centered cubic (fcc) Ni-Fe-W solid-solution matrix. The average tungsten grain size generally varies from 20 to 60 μm, mechanical properties such as strength and ductility are low due to the coarse tungsten grain microstructure. Therefore, material researchers have been investigating and exploring new sintering technology to reduce grain size and refine microstructure to improve mechanical properties, such as employing mechanical alloying to increase powder activation and decrease sintering temperature [4], refining grain size by rare earth additions [5], plasma spraying [6], and laser sintering [7]. To this end, most researchers have directed particular focus towards advanced sintering techniques, such as spark plasma sintering (SPS) [8–11] and wave sintering [12] to explore possible further improvements that can be offered by these methods on the mechanical properties of WHAs.

SPS, often referred to as field assisted sintering technique (FAST) or pulsed electric current sintering (PECS), is a newly arising sintering technique that employs a pulsed direct current (DC) to powders subjected to a modest applied pressure (<100 MPa). High electrical current application enables a fast heating rate (up to 1000 °C.min^{-1}), resulting in a very short sintering cycle, typically a few minutes for full densification of both conductive and nonconductive powders [13,14]. In such a case, a high densification rate is favoured whereas coarsening induced by surface diffusion is minimized, and then grain growth can be suppressed. Moreover, it is stated that SPS can offer other benefits, such as partial oxide film elimination, adsorbed gas release and surface activation of powder particles [15,16]. Recently, the SPS technique has been successfully used to prepare tungsten heavy alloys [17-19]. These features elevate the potential of SPS for wide spread application and comprehensive research in the field of materials.

Given the limitations of the die, the spark plasma sintered samples investigated by some researchers is a cylindrical alloy with a 20 mm diameter [20,21], such a small size presents difficulties in preparing suitable samples for measuring physical properties, such as tensile properties. Even more importantly, in real life applications, for national defence [22], aviation, and civil industries [23], much larger materials are required for these applications in the case of materials fabricated using the sintering method. Preparing much larger samples (>40 mm diameter) presents a difficulty when using SPS in getting homogenous properties within the samples due to poor heat distribution as the sample size gets bigger. Although, the SPS method has several advantages that distinguish it from the traditional sintering methods such as hot pressing and sintering of pre-compacted billets without pressure. Certain disadvantages of the standard SPS/FAST technology are observed (**Fig. 1(a)**), especially when sintering bigger samples, such as radial thermal gradient by thermal drain to the outside or non-heating of the material by too low electrical conductivity. Radial thermal gradient results in inhomogeneous radial microstructures. In the new hybrid spark plasma sintering system (HHPD-25 from FCT Sytem GmbH Germany) radial thermal gradient are eliminated, as the material can be heated additionally and/or exclusively by induction/resistance heating beside heating by pulsed direct current passage (**Fig. 1(b)**) [24]. Significant increase of sintering activity for certain materials by hybrid heating (combination of SPS/FAST technology + resistance/induction heating) could be proved offering homogeneous radial densification. This will result in considerably shorter cycle time and production time. Considering that this is a new technology, WHAs fabricated by this technology has not been reported in the literature, including the advantages offered by this new technology when fabricating samples larger than 40mm. Thus, the mechanical properties and microstructural evolution of 93W-4.9Ni-2.1Fe alloys sintered by the standard SPS/FAST technology compared to those sintered by the hybrid technology will be investigated in this paper.
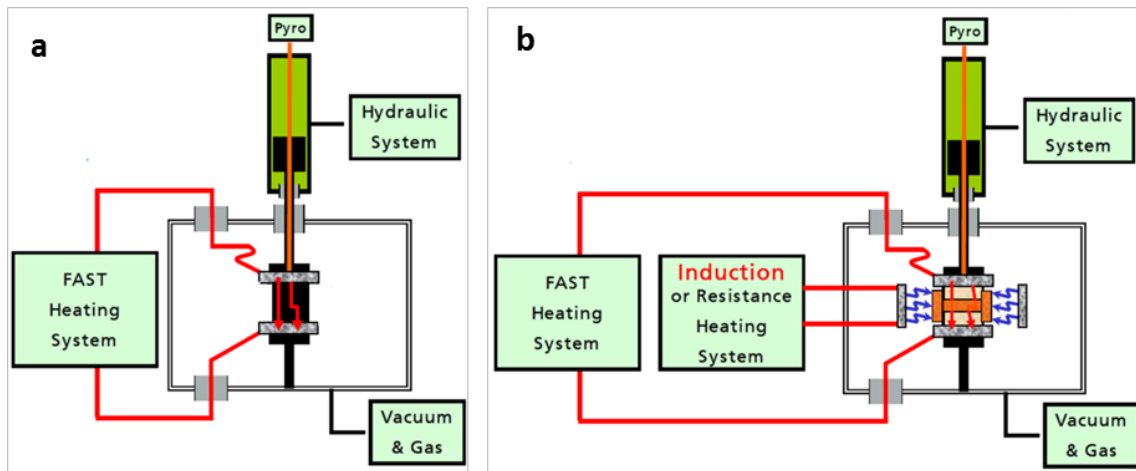
Fig. 1. Schematic of the Spark Plasma Sintering apparatus: a) standard SPS/FAST technology and b) hybrid heating (combination of SPS/FAST technology + resistance/induction heating) [24].

2. Experimental procedure

2.1. Powders preparation

Commercial tungsten, nickel and iron elemental powders were selected for this study. The characteristics of the raw powders are shown in **Table 1**. W, Ni, and Fe powders were weighed accurately to make up a desired stoichiometric composition of 93.0%W-4.9%Ni-2.9%Fe (wt%). Prior to mixing, the morphology of the powders was examined with a field emission scanning electron microscopy (FESEM, JSM-7600F, Jeol, Japan) equipped with energy dispersive X-ray spectrometer (EDS). **Fig. 2 (a) to (c)** shows the SEM morphology of the three as-received powders. The tungsten powder is rounded and spherical in shape, typical of atomized powders, while nickel powder is agglomerated. The three powders were mixed using the Turbula Shaker Mixer T2F in the mass ratios (93%W-4.9%Ni-2.1%Fe (wt%)). An optimum mixing speed of 49 rpm and mixing time of 5h were used. A 250 ml cylindrical plastic vessel with a powder fill level of 10% was loaded axially, placed in the mixing chamber and subjected to translational and rotational motions. The mixing was carried out in a dry environment. The morphology of the mixed powders in shown in **Fig. 2(d)** with a homogenous distribution.

Table 1: Characteristics of the raw powders used to prepare tungsten heavy alloys.

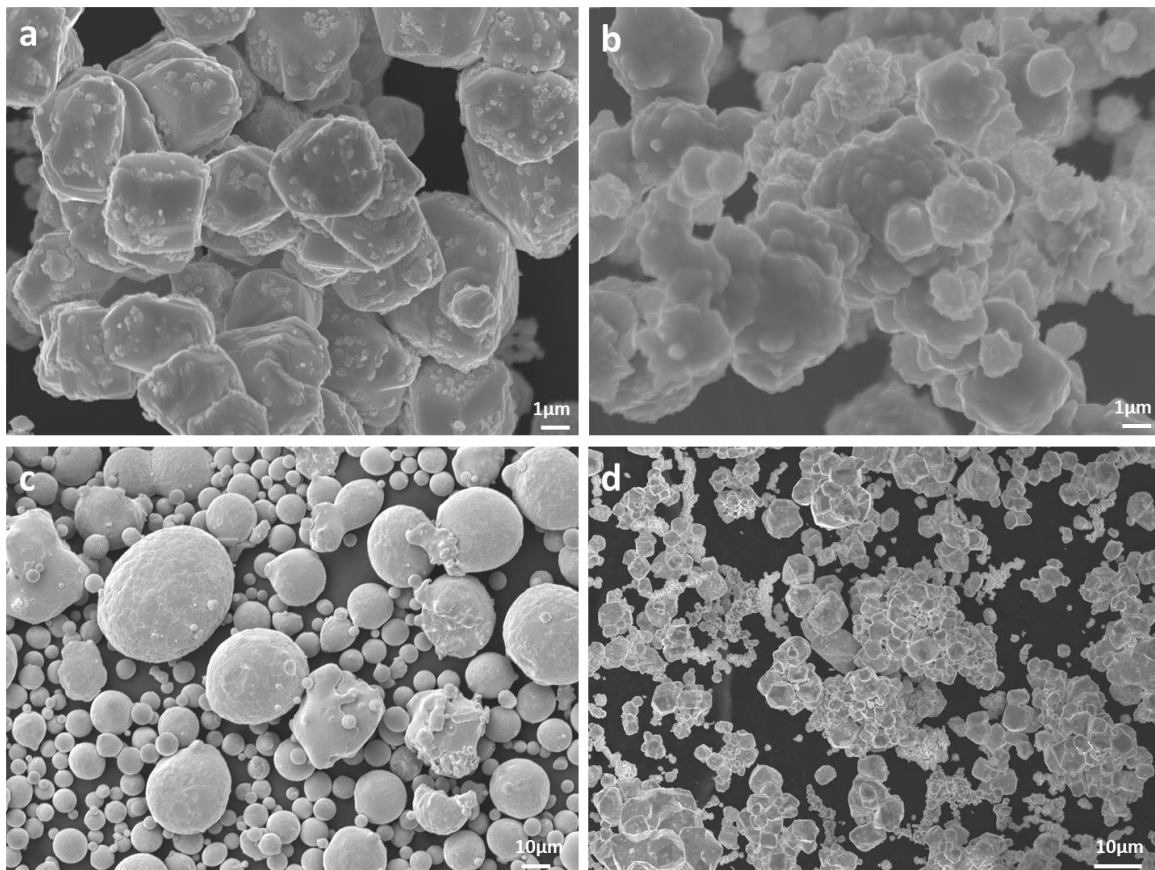| Elemental powder	Purity (%)	Particle size (µm)	Main impurity (wt.%)			
			C	O	P	N
W	99.9	<5	0.002	0.07	0.0008	-
Ni	99.5	<3	≤0.25	≤0.11	0.0003	-
Fe	99.5	<70	≤0.1	≤0.3	-	≤0.1

Fig. 2. SEM morphology of the as-received: (a) Tungsten, (b) Nickel (c) iron, and mixed powders.

2.2. Sintering

The mixed powders were sintered by SPS (HHPD-25 from FCT Syteme GmbH Germany) in a 60 mm and 30 mm-inner-diameter graphite die. Graphite foils of 0.2 mm thickness were placed between the punches and the powders, and between the die and the powders for easy removal and significant reduction of temperature inhomogeneities. In addition, the exterior of the die was covered by a porous graphite felt with thickness of ~10 mm, which was used as a thermal insulation to reduce the radiation loss and possible temperature gradient [25,26]. Sintering was performed in vacuum and a constant pressure of 30 MPa was applied from the

beginning of the heating step to the end of the dwell. For all the sintering experiments, the heating from room temperature to 600°C was controlled by a preset heating program and completed within 4 min, at a heating rate of 150°C/min. From 600°C to the desired temperature, heating rate was 100°C/min. When the required temperature was reached, the electric current was shut off, the applied stress released, and the specimens were immediately cooled down in the furnace. The sintering temperature was measured by an optical pyrometer which was implanted in the SPS apparatus at 3 mm from the top of the sample surface. Discs of 30 and 60 mm diameter of approximately 5 mm in height were produced. The 30 mm discs were produced for the purpose of optimisation and for further comparison with the 60 mm discs.

2.3. Sintered relative density and microstructural characterization

All of the sintered specimens were ground and polished to remove any surface graphite contamination. Then the sintered density was determined by the Archimedes principle. The relative density was calculated with reference to the theoretical density (18.5 g.cm^{-3}) of the starting powders constituents using the rule of mixtures. The microstructure of specimens taken from the polished surface or fracture surfaces at cross sections (parallel to the acting force) of the sintered bodies was examined by SEM (FESEM, JSM-7600F, Jeol, Japan) incorporated with an EDX detector (Oxford X-Max) with INCA X-Stream2 pulse analyzer software, and Back Scattered Electron detectors. The INCA analyzer software was set to 70 seconds acquisition time and at a process time of 2s. The polished specimens were chemically etched with a solution of 6 g potassium ferricyanate and 0.5 g potassium hydroxide in 50 ml of distilled water to observe the microstructure and measure the tungsten grain size. Focus was given on studying the microstructure at different regions along the cross section. To avoid the influence of near-surface effects and some other uncertain factors, only the cross section of the specimen was used for examination. The phases present in the sintered specimen were characterized by X-ray diffraction (XRD) using a PANalytical Empyrean model with Cu Kα radiation and analyzed using Highscore plus software. The XRD analysis was carried out on the section perpendicular to uniaxial pressed direction.

2.4. Mechanical property measurement

The Vickers microhardness ($HV_{0.1}$) at room temperature were measured by a Vickers' microhardness tester (Future-tech) at a load of 1.0 kg and dwell time of 10s and the test result for each sample was the arithmetic mean of ten successive indentations with standard deviations. A Tinius Olsen system (London) measured the bending strength of the sintered alloys, of specimens of $16.00 \times 5.00 \times 2.00$ mm^3 with a loading rate of 0.05 mm/min. The bending strength σ_{bb} is calculated by:

$$\sigma_{bb} = 3FL/2bh^2 \qquad\qquad 1$$

where F is the maximum bending force, L is the span between supporting points which is chosen as 10 mm in the present investigation, b is the width of specimen (5 mm), and h is the thickness of specimen (2 mm).

3. Results and Discussion.

3.1 Densification and Microstructural variations

3.1.1 Density measurement

Comparison of the sintered density for the different conditions is shown in **Fig. 3**. Sintered densities close to theoretical one were achieved for the 30 mm - SPS and HSPS samples, followed by the HSPS, with the least being the 60 mm – SPS sample. Past research has shown densification is a prerequisite for adequate mechanical properties [27-29]. In this, during the SPS and HSPS process, to ensure that the melted matrix phase was not squeezed out from the die cavity, the liquid-phase sintering is performed for only a short moment. The lower relative density of the 60 mm – SPS sample is not surprising due to the additional heating source in the case of HSPS which suggest uniform distribution opf heat resulting in improved densification and homogeneous microstructure throughout the whole sample.
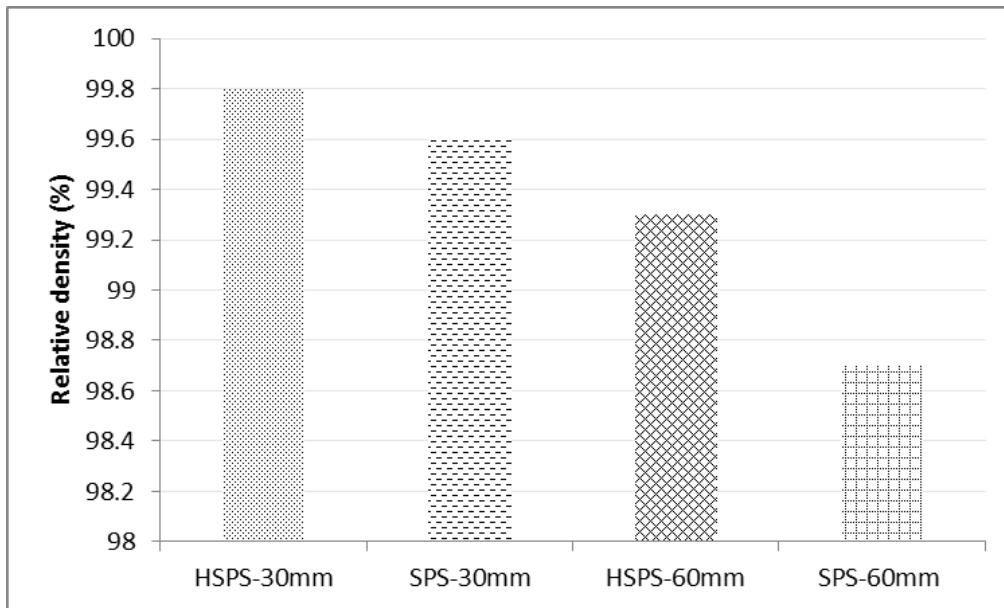
Fig. 3. Effect of sintering technique and sample diameter on the relative density of W-Ni-Fe alloys.

3.1.2 Microstructural characterization

The progressive evolution of microstructures in different regions of the sample manufactured using SPS and HSPS for 60 mm is given in **Fig. 4**. All the microstructures were taken at similar positions and low magnification (500x) in order to ensure that the grains distribution is captured. There are relatively different arrangements of the W grains, which respectively designate the variation in densification. It is noted that at the edge of the sample for the SPS sample (**Fig. 4(a)**) the microstructure is inhomogeneous as opposed to the HSPS sample (**Fig. 4(b)**). During SPS of large samples there is a tendency of having a radial temperature distribution. Because of the low sintering temperature, the samples sintered via SPS had a much lower edge temperature, thus probably less melting of Ni took place, and the sample at the edge was majorly fabricated by solid-phase sintering, consequently its microstructure distributes inhomogeneously. This suggests tremendous changes of hardness in various parts of the samples as a result of the inhomogeneous microstructure. Meanwhile, the microstructure in **Fig. 4(b)** has a better distribution than **Fig. 4(a)** indicating a better densification and more evidence of sintering necks. The sintering necks between the tungsten grains would promote the diffusion between tungsten grains and contribute to the densification of the alloy [30]. Although the sintering necks are also observed in **Fig. 4(a)**, this is more dominant in **Fig. 4(b)** where W particles can be observed with a higher packing density, and an increase in the number of necks and their size which indicates an improve

sintering. As pointed out by Song et al. [31], neck growth depends on the local distribution of the current density and a self-adjusting mechanism leads to a final homogeneous distribution of necks. In SPS the high local temperature gradients enhances consolidation through thermal diffusion [32] and the higher sintering temperature, the higher overheating. With a better temperature distribution with respect to the centre of the sample (**Fig 4(e and f)**), diffusion was enhanced and densification was accelerated, which resulted in a homogenous microstructure and thereof better densification. The mechanical properties are expected to be greatly improved in the HSPS sample due to the homogeneous distribution of the microstructure of component phases considered. Based on this observation it is apparent that the relative density for the HSPS sample is higher than that of SPS, and these results illustrate that tungsten grains growth, pores reduction and density improvement are all simultaneous processes. For both conditions, the packing density of the W grains is improved as the core of the sample is approached ((**Fig. 4(g and h)**).

It is believed that particularly for the SPS sample, the core predominantly experienced liquid phase sintering as compared to the edge of the sample which was at a slightly lower temperature. During the liquid phase sintering period, there was a cascade of rearrangement and solution-reprecipitation events of the tungsten atoms which played a significant role in the process of grain coalescence and growth [33], resulting in a higher packing density of the grains and a homogenous distribution of the grains in the core ((**Fig. 4(g)**). Solution-reprecipitation is dominant when the solid is soluble in the liquid. Tungsten atoms are dissolved into the liquid phase, preferentially from higher energy regions, including asperities, convex points, and small tungsten grains. And the dissolved tungsten atoms diffuse in the liquid phase and reprecipitate on concave regions or larger grains, which lead to the disappearance of small tungsten grains and growth of large tungsten grains (**see Fig. 5(a)**). Meanwhile, neighbouring tungsten grains bond together and coalesce into larger grains. **Fig. 5** is a higher magnification of the core of the sample which indicates the presence of sintering necks in both cases, however the SPS sample (**Fig. 5(a)**) is dominated by larger grains, while the HSPS sample (**Fig. 5(b)**) sintering necks exist between smaller and larger grains. An overview of the HSPS compared to the SPS clearly shows the latter has both smaller and larger grains, while the former had mostly larger grains and an inhomogenously distributed microstructure. The large grains in the SPS sample are thought to be due to a much higher localized overheating, compared to the actual measured temperature of 1350°C. For the 30 mm, SPS and HSPS samples, no variations were observed from the edge to the core of the

microstructure. Representative SEM micrographs for both conditions are shown in **Fig. 6**. The grains packing density was similar to the HSPS 60 mm sample (**Fig 4(h)**). The results from the composition analysis are listed in **Table 2**. Besides the presence of a minimal amount of Ni and Fe, the white structure is mainly W. A typical high resolution image for the HSPS -30 mm in BSE is shown in **Fig. 7** and this indicated only two contrast changes, similar to the low magnification images and thus no presence of a third phase was observed.
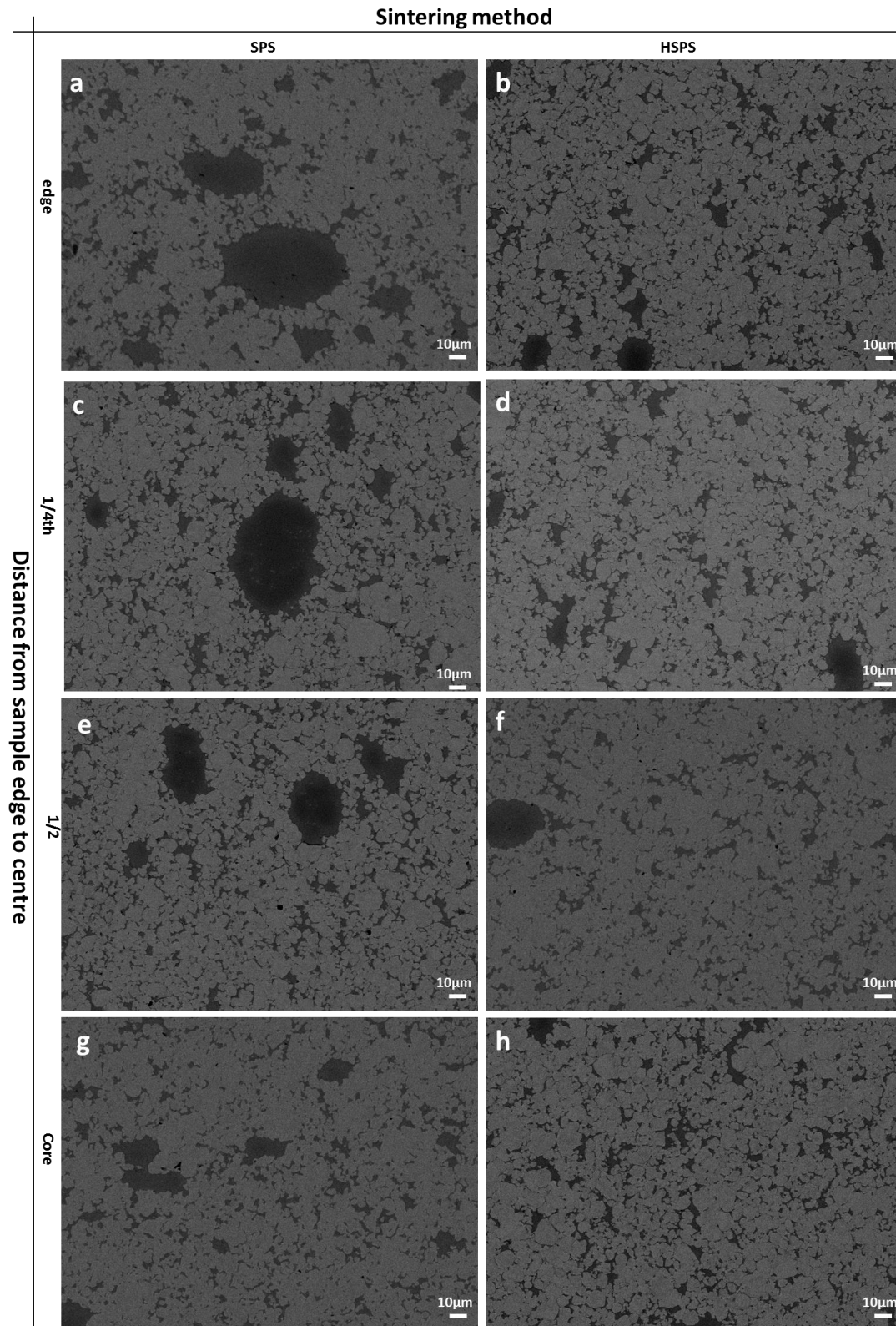
Fig. 4. SEM micrographs of the 93W–4.9Ni–2.1Fe alloy showing the microstructural evolution of the samples from the edge to the core sintered with different conditions: Left side - SPS and right side – HSPS, both for 60mm.
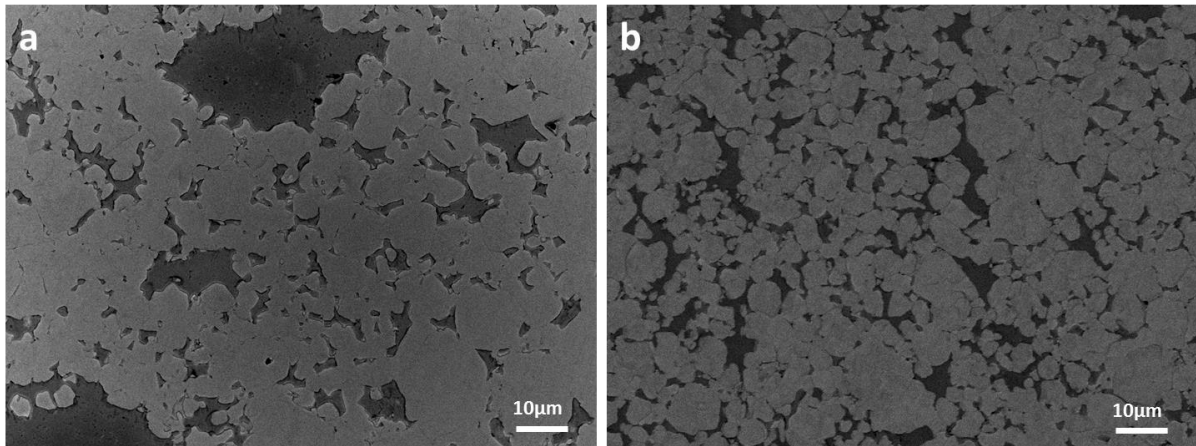
Fig. 5. SEM micrographs of the 93W–4.9Ni–2.1Fe alloy sintered with different conditions: (a) SPS-60mm and (b) HSPS -60mm showing evidence of sintering necks.
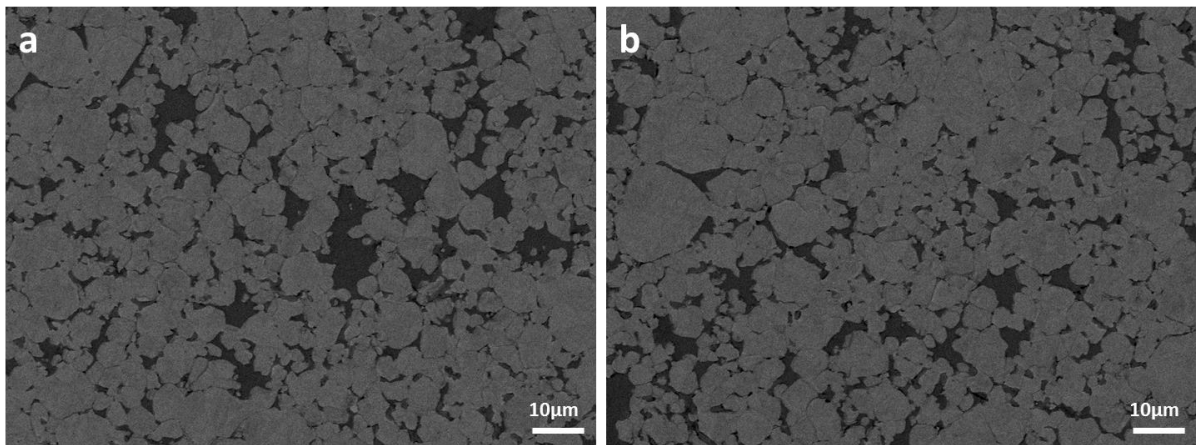

Fig. 6. SEM micrographs of the 93W–4.9Ni–2.1Fe alloy sintered with different conditions: (a) SPS-30mm and (b) HSPS -30mm showing evidence of sintering necks.
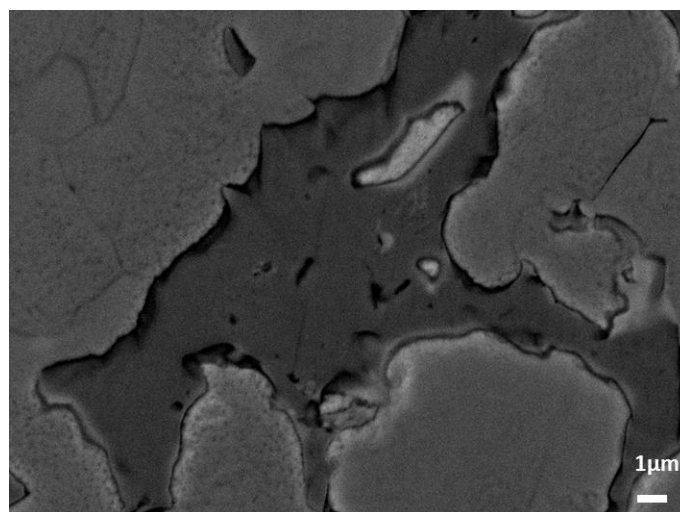

Fig. 7. SEM high magnification micrograph of the 93W–4.9Ni–2.1Fe 30mm-HSPS alloy.

Table 2: Phase compositions of W–4.9Ni–2.1Fe alloys fabricated by HSPS and SPS.

Alloy	Phase	Element composition (wt.%)		
		W	Ni	Fe
HSPS-30mm	W	96.5	2.2	1.4
	Ni,Fe	25.2	46.8	28.0
SPS-30mm	W	95.5	2.6	1.9
	Ni,Fe	22.4	48.0	29.6
HSPS-60mm	W	94.9	3.2	1.9
	Ni,Fe	24.2	45.6	30.2
SPS-60mm	W	95.8	2.8	1.4
	Ni,Fe	26.1	44.5	29.4

3.2 Mechanical properties and fractography

Fig. 8 shows the micro hardness profile from edge to centre point of the sample for W-4.9Ni-2.1Fe fabricated by SPS and by HSPS for the 60 mm samples at 1350°C. **Fig. 8** depicts the micro hardness variation on the cross-sections of the two samples. Generally, the hardness increased with increased distance from the edge. The variation in micro-hardness, which is similar to that of grain size variation from edge to the centre, is more obvious in the SPS sample. The bigger difference between the microstructure at the edge and centre especially for the SPS sample is attributed to non-uniform heat distribution resulting in poor densification at the edge and inhomogeneous microstructure that led to tremendous changes in hardness on various parts of the samples. The higher hardness at the centre of the sample relative to the edge suggest the formation of a certain amount of liquid phase which gives rise to inhomogenous microstructure. The hardness HSPSed material is approximately 30% higher than that of SPS at the edge of the sample, the reason being the near full densification of the former. The higher hardness values of the sample prepared by HSPS confirm that radial temperature fluctuations are minimised and most of the sample is consolidated by liquid phase. **Fig. 9** shows a plot of the average hardness of the samples produced by SPS and HSPS. The microhardness of HSPS and SPS sample of 60 mm and 30 mm are very close to each other, this is due to the fact for the HSPS system the 60 mm sample temperature distribution ensures good consolidation. , The good densification of the SPS 30 mm sample is as a result of the small size of the sample which allows only small radial temperature

fluctuations. Compared to the HSPS 60 mm sample, the SPS 60 mm has a much smaller hardness confirming the earlier observations in **Fig. 8**.
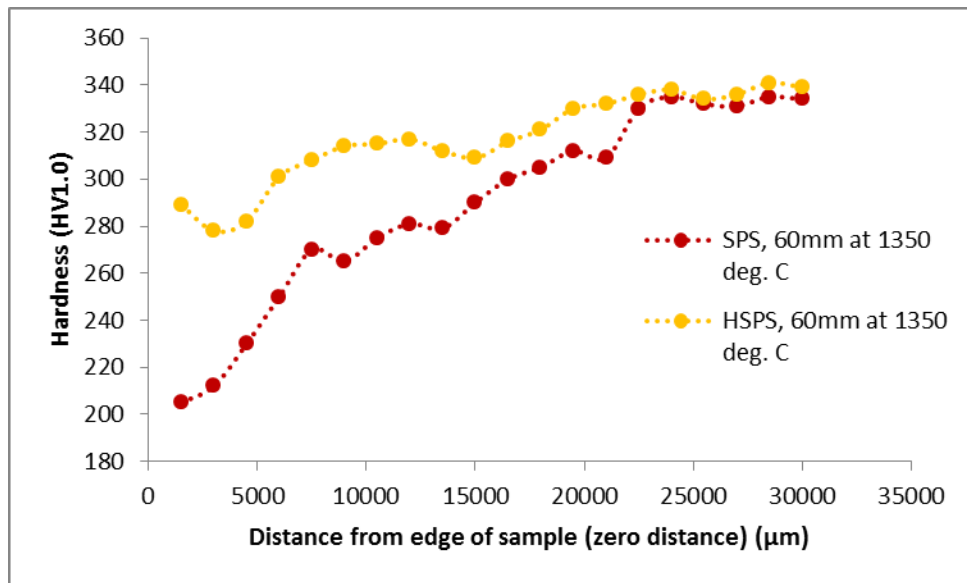

Fig. 8. The variation of micro-hardness in from the edge of the sample to the centre for W-Fe-Ni fabricated by SPS and by HSPS for the 60mm samples at 1350°C.
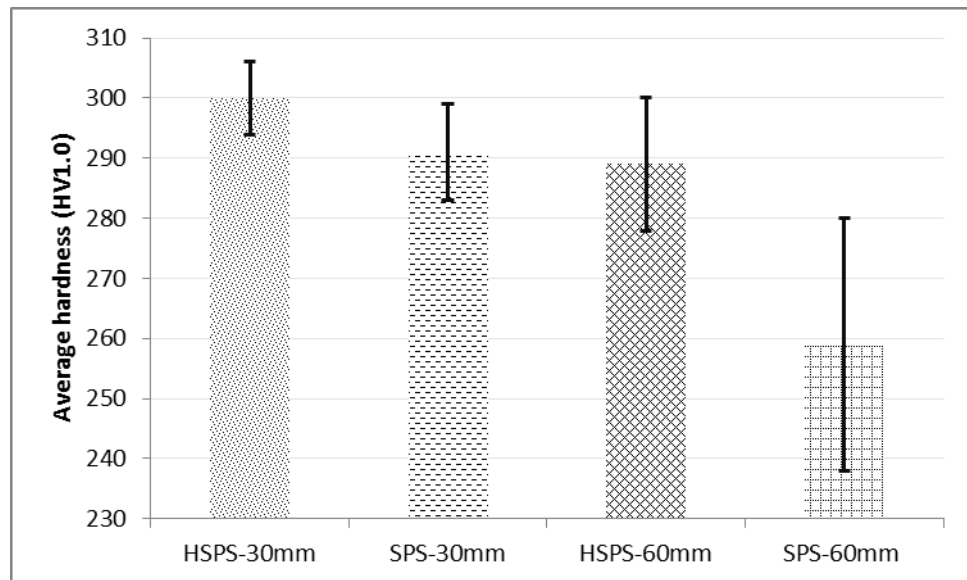

Fig. 9. Average Vickers' microhardness (HV1.0) for samples fabricated using HSPS and SPS for 30 and 60mm diameters.

The densities and mechanical properties of the alloys after sintering are recorded in Table 3. Comparing the average microhardness values obtained in this study for 30 mm-SPS, -HSPS and 60 mm-SPS and –HSPS, with the hardness value obtained by Yang et. al [34] as shown in Table 3, it could be seen that there little differences in hardness between the samples obtained in this study and samples produced by Yang et al [34]. The relative density for

HSPS-30 mm is about 0.998, which is relatively higher to other refs [35, 37,38] expect for ref [36] which was attributed to enhanced sintering resulting from mechanical alloying.

Table 3. Variation of relative density and hardness in this study versus those of other W–Ni–Fe alloys obtained from the literatures.

Alloy	Element composition (wt.%)			Relative density	Hardness Value (HV)
	W	Ni	Fe		
HSPS-30mm	96.5	2.2	1.4	0.998	300
	25.2	46.8	28.0		
SPS-30mm	95.5	2.6	1.9	0.996	290
	22.4	48.0	29.6		
HSPS-60mm	94.9	3.2	1.9	0.993	289
	24.2	45.6	30.2		
SPS-60mm	95.8	2.8	1.4	0.987	259
	26.1	44.5	29.4		
ref [34]	93	4.9	2.1Fe		286
ref [35]	93	5.6	1.4	0.995	
ref [36]	93	5.6	1.4	0.999	
ref [37]	93	5.6	1.4	0.985	
ref [38]	91	7	1.5	0.994	

Fig. 10 represents the effect of sintering method and sample size on the bending strength of W-4.9Ni-2.1Fe alloys. The 60 mm-SPS has a slightly lower bending strength than the other 3 samples which have a similar bending strength. The change of trend in the bending strength of the sampless is closely related to the variations in microstructure. Thus in order to explain these variations on the bending strength, the bending fracture morphology needs to be assessed first. **Fig. 11** shows the bending fracture morphology of the W-4.9Ni-2.1Fe alloys for the different sizes and sintering methods, obtained from the core of each sample. Comparing Fig. **11(a)** to the rest of the samples (**Fig. 11 (b to d)**), the grain structure is very inhomogeneous with bigger and very fine grains. Aside from the small grain region in **Fig. 11(a)**, the rest of the grains are much bigger than the rest of the alloys **(Fig. 11 (b to d)**, which is similar to the observation made in the polished surface analysis. The shape of the larger grains is also very irregular compared to the other samples. The finer grain region has spherical W grains (shown in higher magnification in **Fig. 11(b)**) which were not observed in the rest of the alloys. It is important to note that the finer grains could not have been observed on the polished surface possibly because it was a layer not within the cross section cut, while the fracture surface exposed it. Within the smaller grains region the fracture mode is mainly

the peeling off of W grains; and a small amount of W grains have cleavage fracture as illustrated within the highest magnification insert. With the peeling of grains, the mechanical properties of the alloys are lower. For the rest of the alloys, no peeling off of grains is observed, and the intergranular fracture of the W grains and the ductile tearing of the binding phase become the main fracture modes, and a few cleavage of the W grains occur. Therefore, the mechanical properties of the rest of the samples are improved compared to **Fig. 11(a)**. In **Fig. 11(a)**, given the significant increase in W grain size, the contact area of the W-W grains expands, producing larger fracture sources, with also visible micropores occurring within the W-W grain interfaces, thereby weakening the alloy strength. Compared to the rest of the alloys, the 60 mm-SPS sample (**Fig. 11(a)**) has the largest micropores, which are not observed on the rest of the alloys. With increasing W grain size, the total grain-boundary area decreases and the stress in the unit grain-boundary area increases under the same loads (compared to the rest of the alloys). The observed micropores in **Fig. 11(a)** could be due to the fact that the core of the sample has a low binding phase (Ni) as the alloy in the core of the sample could have experienced much higher temperature than the rest of the alloy. According to Wang et al. [35], a high vacuum sintering temperature enables easy volatilization of the binding phase (especially Ni) [34]. This convenience may be the reason for the slight decrease in the relative density and bending of the 60 mm-SPS alloys. From this highlighted observations, the fractography results (**Fig. 11**) are in agreement with the low bending strength of 60 mm-SPS compared to the other 3 samples (**Fig. 10**)
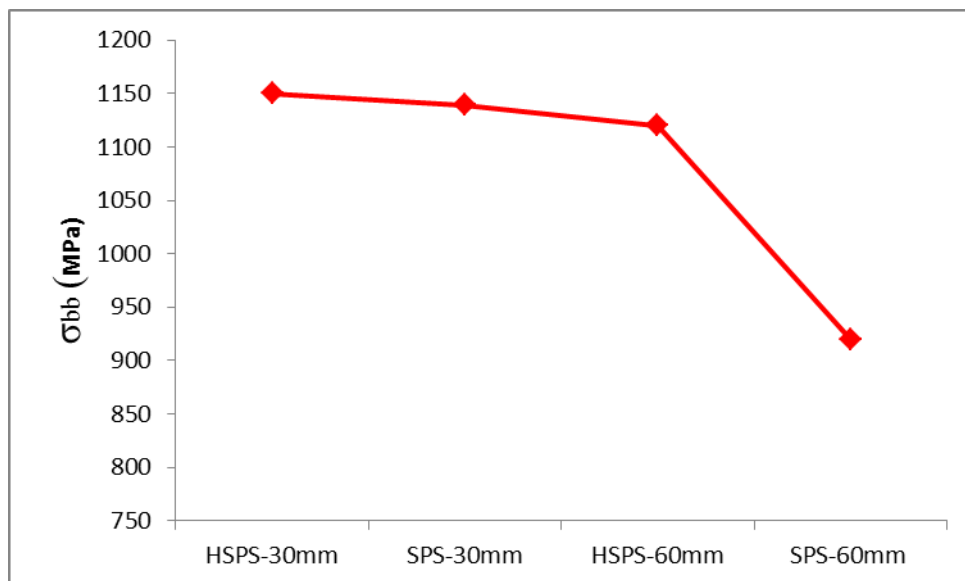

Fig. 10. Effect of sintering method and sample size on the bending strength of W-Ni-Fe alloys
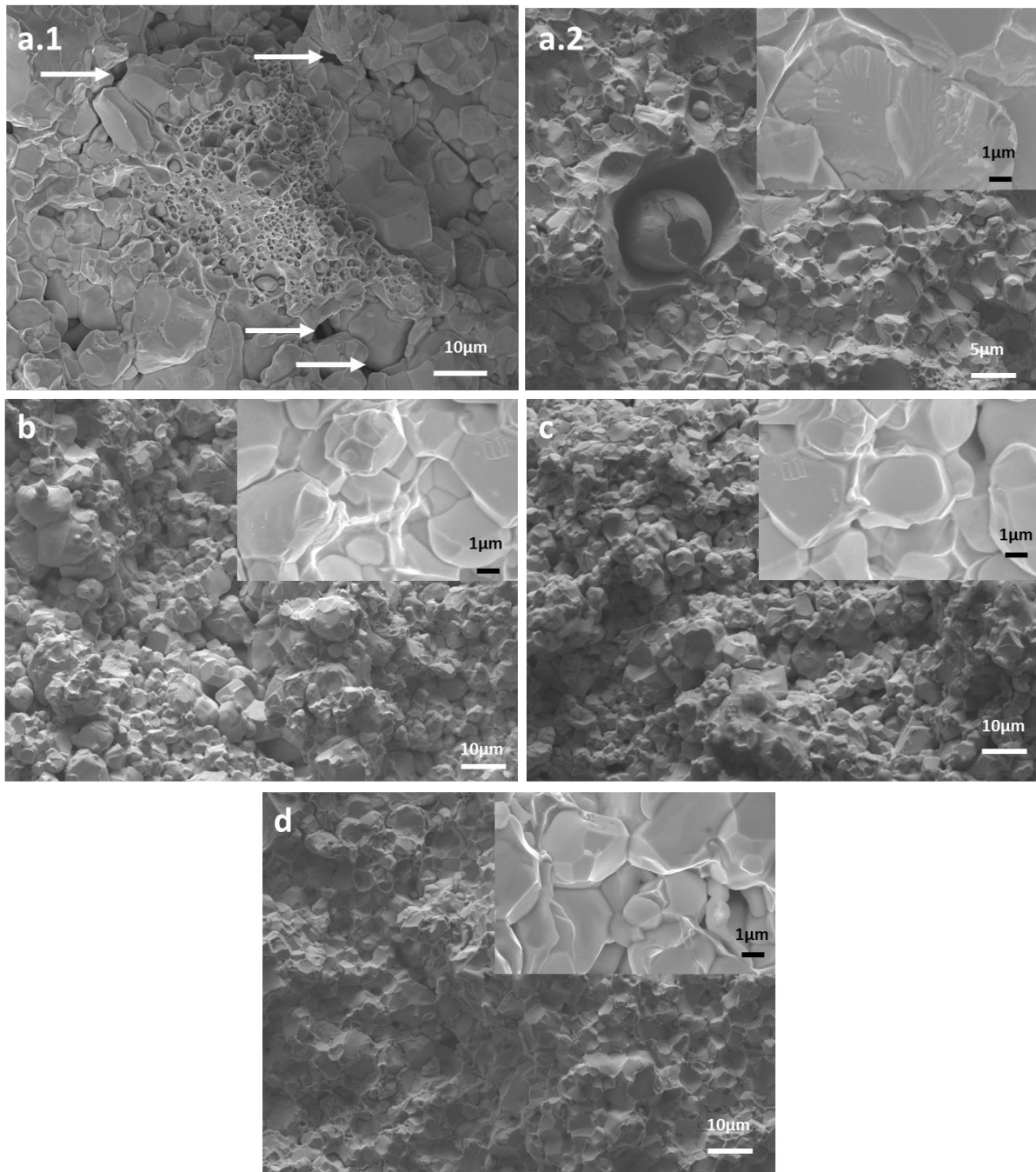
Fig. 11. Fracture morphology of W-Ni-Fe alloy sintered at 1350°C for: a) 60 mm-SPS, b) 60 mm-HSPS, c) 30 mm-SPS and d) 30 mm-HSPS.

4. Conclusions

93W-4.9Ni-2.1Fe heavy alloys using blended powders were sintered by SPS and HSPS with 30 mm and 60 mm diameters. The microstructure and mechanical properties of the alloys were investigated. The conclusions are summarized as follows:

(1) The 60 mm-SPS sample showed a variation of the tungsten packing density and grain size, while for the 60mm-HSPS minor variation were observed, confirming the minimized radial temperature fluctuations.

(2) Near full densification was achieved for the 30 mm-HSPS and SPS samples followed by 60 mm-HSPS, while the 60 mm-SPS sample had a low relative density of 98.7%.

(3) A micro hardness profile for the 60 mm SPS and HSPS sample was carried out, and the SPS sample had the greatest changes, even though the hardness increased for both samples towards the core of the sample. This was explained by the variation in the microstructure, as seen with changes in tungsten grain size and packing density, which was more obvious in the SPS sample. No variations were observed in the 30 mm samples. The average hardness values were similar for the 30 mm SPS/HSPS samples, with the 60 mm-HSPS being third highest, while the 60 mm-SPS was the least.

(4) The bending strength of 60 mm-SPS (920 MPa) was lower than that of 60 mm-HSPS (1115 MPa), this indicating that the strength is dependent on microstructural parameters such as tungsten grain size and packing density and also the presence of micropores. In the 60 mm-SPS two fracture modes were observed, intergranular fracture of bigger grains and peeling of the smaller ones which lowered the properties. The average grain size of the 30 mm and 60 mm-HSPS alloys was ~5µm, while that of the 60 mm was dominated by larger grain sizes (~10µm) with less regions of finer grains (5 to 1µm).

This work has shown that HSPS has the beneficial effect of improving or maintaining comparable properties (density, hardness and binding strength) for larger samples.

REFERENCES

[1] Cai WD, Li Y, Dowding RJ, Mohamed FA, Lavernia EJ. A review of tungsten-based alloys as kinetic energy penetrator materials. Rev. Particulate Mater. 1995;3: 71–131.

[2] German RM. Critical developments in tungsten heavy alloys. In: Bose A, Dowding RJ, editors, Tungsten and tungsten alloys. Princeton (NJ): MPIF, 1992;3–13.

[3] Shudong L, Jianhong Y, Ying Li G, Yuandong P, Liya, Junming LR. Microwave sintering W-Cu composites: Analyses of densification and microstructural homogenization. J. Alloys Compds 2009;473:5–9.

[4] Test HJ, Mechanical alloying process of 93W-5.6Ni-1.4Fe tungsten heavy alloy. J. Mater. Process Technol 1997;63:292–7.

[5] Jinglian F, Tao L, Huichao V, Denglong W. Preparation of fine grain tungsten heavy alloy with high properties by mechanical alloying and yttrium oxide addition, J Mater Process Technol 2008;208:463–9.

[6] Jiˇrʹı M, Yoshie K, Vladimʹır W. Plasma sprayed tungsten based coatings and their performance under fusion relevant conditions, Fusion Eng. Des 2005;75:395–399.

[7] Bagchi TP, Arvind Kumar N, Sarma B, Maitra N. Problem solving in sintering of tungsten heavy alloy product-a case study, Mater. Chem. Phys 2001;67:111–119.

[8] Grigoriev EG, Rosliakov AV. Electro-discharge compaction of WC‑Co and W‑Ni‑Fe‑Co composite materials. J. Mater. Process. Technol 2007;191:182–184.

[9] Chuvil'deev VN, Moskvicheva AV, Baranov GV, Nokhrin AV, Lopatin YG, Belov VY, Blagoveshchenskii YV, Shotin SV. Superhard nanodisperse tungsten heavy alloys obtained using the methods of mechanical activation and spark plasma sintering. Tech. Phys. Lett 2009;35:1036–1039.

[10] Chuvil'deev VN, Moskvicheva AV, Nokhrin AV, Baranov GV, Blagoveshchenskii YV, Kotkov DN, Lopatin YG, Belov VY. Ultrastrong nanodispersed tungsten pseudoalloys produced by high-energy milling and spark plasma sintering. Dokl. Phys 2011;56:109–113.

[11] Hu. K, Li XQ, Qu S.G, Li YY. Spark-Plasma Sintering of W-5.6Ni-1.4Fe Heavy Alloys: Densification and Grain Growth. Metall. Mater. Trans. A 2013;44:923–933.

[12] Upadhyaya A, Tiwari SK, Mishra P. Microwave sintering of W‑Ni‑Fe alloy. Scr. Mater 2007;56:5–8.

[13] Groza J.R. Met. Field activation provides improved sintering. Powder Rep 2000;55:16–18.

[14] Kandukuri S. A FAST winner for fully dense nano powders. Met. Powder Rep 2008;63:22–27.

[15] Anderson K.R, Groza J.R, Fendorf M, Echer C.J. Surface oxide debonding in field assisted powder sintering. Mater. Sci. Eng. A 1999;270:278–282.

[16] Groza JR, Zavaliangos A. Sintering activation by external electrical field Mater. Sci. Eng. A 2000;287:171–177.

[17] Hu K, Li X, Yang C, Li Y. Densification and microstructure evolution during SPS consolidation process in W-Ni-Fe system. Trans. Nonferrous Met. Soc. China 2011;21:493–501.

[18] Ding L, Xiang DP, Li YY, Li C, Li JB. Effects of sintering temperature on fine-grained tungsten heavy alloy produced by high-energy ball milling assisted spark plasma sintering. Int. J. Refract. Met. Hard Mater. 2012;33:65–69.

[19] Xiang DP, Ding L, Li YY, Li JB, Li XQ, Li C. Microstructure and mechanical properties of fine-grained W‑7Ni‑3Fe heavy alloy by spark plasma sintering. Mater. Sci. Eng. A 2012;551:95–99.

[20] Ding L, Xiang DP, Li YY, Zhao YW, Li JB, Phase. Microstructure and properties evolution of fine-grained W–Mo–Ni–Fe alloy during spark plasma sintering, Materials and Design 37 (2012) 8–12.

[21] Li Y, Hu K, Li X, Ai X, Qu S. Fine-grained 93W–5.6Ni–1.4Fe heavy alloys with enhanced performance prepared by spark plasma sintering, Materials Science &Engineering A 2013;573:245–252.

[22] Upadhyaya A. Processing strategy for consolidating tungsten heavy alloys for Ordinance applications. Mater Chem Phys 2001; 67: 101–110.

[23] Humail IS, Akhtar F, Askari SJ, Jokhio MT, Qu XH, Tensile behavior change depending on the varying tungsten content of W–Ni–Fe alloys. Int. J. Refract. Met. Hard Mater 2007;25:380–385.

[24] New hybrid system on the market, http://www.fct-systeme.de/fr/news/detail/~id.9~archiv.1~page3/New-hybrid-system-on-the-market.html (accessed May 12, 2015).

[25] Räthel J, Herrmann M, Beckert W. Temperature distribution for electrically conductive and non-conductive materials during Field Assisted Sintering (FAST), J. Eur. Ceram. Soc 2009;29:1419–1425.

[26] Zavaliangos A, Zhang J, Krammer M, Groza JR. Temperature evolution during field activated sintering, Mater. Sci. Eng. A 2004;379:218–228.

[27] Kang TK, Henig E-T, Kaysser WA, Petzow G. Modern developments in powder metallurgy. Hausner H.H, Antes HW, Smith GD eds. Metal Powder Industries, Princeton, NJ, 1981;14:189-203.

[28] Churn K-S, Yoon DN. Pore Formation and Its Effect on Mechanical Properties in W—Ni—Fe Heavy Alloy. Powder Met 1979;22:175-178.

[29] Googin JM, Harper WL, Neeley AC, Phillips LR. Development of ductile tungsten alloys," Report Y-1364, Y-12 Plant, Union Carbide Nuclear Division, Oak Ridge, TN, August 1961.

[30] Farid A. An investigation on the solid state sintering of mechanically alloyed nano-structured 90W-Ni-Fe tungsten heavy alloy. Int. J. Refract. Metals Hard Mater. 2008; 26:145–51.

[31] Song X, Liu X, Zhang J. Neck formation and self-adjusting mechanism of neck growth of conducting powders in spark plasma sintering. J. Am. Ceram. Soc 2006;89:494–500.

[32] Olevsky EA, Froyen L. Impact of thermal diffusion on densification during SPS. J. Am. Ceram. Soc 2009;92:122-132.

[33] German RM, Pavan S, Seong JP. Review: liquid phase sintering. Mater Sci 2009; 44:1–39.

[34] Yang Y, Lianxi H, Erde, W. Microstructure and mechanical properties of a hot-hydrostatically extruded 93W–4.9Ni–2.1Fe alloy. Mater. Sci. En. A 2006:435–436:620–624.

[35] Li, Y, Hu, K., Li, X., Ai, X, Qu, S. Fine-grained 93W–5.6Ni–1.4 Fe heavy alloys with enhanced performance prepared by spark plasma sintering. Mater. Sci. Eng. A2013: 573:245–252.

[36] Hong, S.H., Ryu, H.J. Combination of mechanical alloying and two-stage sintering of a 93W-5.6Ni-1.4Fe tungsten heavy alloy. Mater. Sci. Eng. A 2003: 344:253–260.

[37] Ryu, H.J., Hong, S.H. Fabrication and properties of mechanically alloyed oxide-dispersed tungsten heavy alloys. Mater. Sci. Eng. A 2003: 363:179–184.

[38] Das, J. Raoa, G.A., Pabi, S.K. Microstructure and mechanical properties of tungsten heavy alloys. Mater. Sci. Eng. A 2010: 527:7841–7847.

[39] Wang YC, Li SK, Wang FC, Luo HZ. Microstructure and Mechanical Properties of 93W-4.9Ni-2.1Fe by Spark Plasma Sintering. The 8th Pacific Rim International Congress on Advanced Materials and Processing.